Polarimetry noise in fiber-based optical coherence tomography instrumentation

Polarimetry noise in fiber-based optical coherence tomography instrumentation

Ellen Ziyi Zhang* **and Benjamin J. Vakoc**

Wellman Center for Photomedicine
Harvard Medical School and Massachusetts General Hospital
40 Blossom Street, Boston, Massachusetts 02114, USA
*zzhang0@partners.org

Abstract: High noise levels in fiber-based polarization-sensitive optical coherence tomography (PS-OCT) have broadly limited its clinical utility. In this study we investigate contribution of polarization mode dispersion (PMD) to the polarimetry noise. We develop numerical models of the PS-OCT system including PMD and validate these models with empirical data. Using these models, we provide a framework for predicting noise levels, for processing signals to reduce noise, and for designing an optimized system.

OCIS codes: (170.4500) Optical coherence tomography; (120.5410) Polarimetry; (260.5430) Polarization; (260.1440) Birefringence; (170.3880) Medical and biological imaging.

References and links

1. D. Huang, E. A. Swanson, C. P. Lin, J. S. Schuman, W. G. Stinson, W. Chang, M. R. Hee, T. Flotte, K. Gregory, C. A. Puliafito, and J. G. Fujimoto, "Optical coherence tomography," Science **254,** 1178–1181 (1991).
2. M. R. Hee, D. Huang, E. A. Swanson, and J. G. Fujimoto, "Polarization-sensitive low-coherence reflectometer for birefringence characterization and ranging," J. Opt. Soc. Am. B **9,** 903–908 (1992).
3. J. F. de Boer, T. E. Milner, M. J. C. van Gemert, and J. S. Nelson, "Two-dimensional birefringence imaging in biological tissue by polarization-sensitive optical coherence tomography," Opt. Lett. **22,** 934–936 (1997).
4. E. Götzinger, M. Pircher, M. Sticker, A. F. Fercher and C. K. Hitzenberger, "Measurement and imaging of birefringent properties of the human cornea with phase-resolved, polarization-sensitive optical coherence tomography," J. Biomed. Opt. **9,** 94–102 (2004).
5. M. Zhao and J. A. Izatt, "Single-camera sequential-scan-based polarization-sensitive SDOCT for retinal imaging," Opt. Lett. **34,** 205–207 (2009).
6. E. Götzinger, M. Pircher, B. Baumann, C. Ahlers, W. Geitzenauer, U. Schmidt-Erfurth, and C. K. Hitzenberger, "Three-dimensional polarization sensitive OCT imaging and interactive display of the human retina," Opt. Express **17,** 4151–4165 (2009). http://www.opticsinfobase.org/abstract.cfm?URI=oe-17-5-4151
7. A. Miyazawa, M. Yamanari, S. Makita, M. Miura, K. Kawana, K. Iwaya, H. Goto, and Y. Yasuno, "Tissue discrimination in anterior eye using three optical parameters obtained by polarization sensitive optical coherence tomography," Opt. Express **17,** 17426-17440 (2009). http://www.opticsinfobase.org/oe/abstract.cfm?URI=oe-17-20-17426
8. C. E. Saxer, J. F. de Boer, B. H. Park, Y. Zhao, Z. Chen, and J. S. Nelson, "High-speed fiber-based polarization-sensitive optical coherence tomography of in vivo human skin," Opt. Lett. **25,** 1355–1357 (2000).
9. B. H. Park, C. Saxer, S. M. Srinivas, J. S. Nelson, and J. F. de Boer, "In vivo burn depth determination by high-speed fiber-based polarization sensitive optical coherence tomography," J. Biomed. Opt. **6,** 474–479 (2001).
10. M. Todorovic, S. Jiao, J. Ai, D. Pereda-Cubin, G. Stoica, and L. V. Wang, "In vivo burn imaging using Mueller optical coherence tomography," Opt. Express **16,** 10279–10284 (2008). http://www.opticsinfobase.org/abstract.cfm?URI=oe-16-14-10279
11. S. D. Giattina, B. K. Courtney and P. R. Herz, M. Harman, S. Shortkroff, D. L. Stamper, B. Liu, d, J. G. Fujimoto and M. E. Brezinski, "Assessment of coronary plaque collagen with polarization sensitive optical coherence tomography (PS-OCT)," Int. J. Cardiol. **107,** 400–409 (2006).

#148363 - $15.00 USD Received 1 Jun 2011; revised 1 Jul 2011; accepted 11 Jul 2011; published 15 Aug 2011

12. S. Nadkarni, M. C. Pierce, B. H. Park, J. F. de Boer, E. F. Halpern, S. L. Houser, B. E. Bouma, G. J. Tearney, "Measurement of collagen and smooth muscle cell content in atherosclerotic plaques using polarization-sensitive optical coherence tomography," J. Am. Coll. Cardiol.**49,** 1474–1481 (2007).
13. J. F. de Boer and T. E. Milner, "Review of polarization sensitive optical coherence tomography and Stokes vector determination," J. Biomed. Opt.**7,** 359–371 (2002).
14. K. Schoenenberger, B. W. Colston, D. J. Maitland, L. B. Da Silva, and M. J. Everett, "Mapping of Birefringence and Thermal Damage in Tissue by use of Polarization-Sensitive Optical Coherence Tomography," Appl. Opt. **37,** 6026–6036 (1998).
15. S. Makita, M. Yamanari, and Y. Yasuno, "Generalized Jones matrix optical coherence tomography: performance and local birefringence imaging," Opt. Express **18,** 854-876 (2010). http://www.opticsinfobase.org/oe/abstract.cfm?URI=oe-18-2-854
16. B. H. Park, M. C. Pierce, B. Cense, and J. F. de Boer, "Optic axis determination accuracy for fiber-based polarization-sensitive optical coherence tomography," Opt. Lett. **30,** 2587–2589 (2005).
17. S. Yun, G. Tearney, J. de Boer, and B. Bouma, "Removing the depth-degeneracy in optical frequency domain imaging with frequency shifting," Opt. Express **12,** 4822–4828 (2004). http://www.opticsinfobase.org/oe/abstract.cfm?URI=oe-12-20-4822
18. P. Leong, and S. Carlile, "Methods for spherical data analysis and visualization," J. Neurosci. Methods **80,** 191–200 (1998).
19. E. Götzinger, M. Pircher, W. Geitzenauer, C. Ahlers, B. Baumann, S. Michels, U. Schmidt-Erfurth, and C. K. Hitzenberger, "Retinal pigment epithelium segmentation by polarization sensitive optical coherence tomography," Opt. Express **16,** 16410–16422 (2008). http://www.opticsinfobase.org/oe/abstract.cfm?URI=oe-16-21-16410
20. N. Vansteenkiste, P. Vignolo, and A. Aspect, "Optical reversibility theorems for polarization: Application to remote control of polarization," J. Opt. Soc. Am. A **10,** 2240–2245 (1993).
21. N. Gisin and B. Huttner, "Combined effects of polarization mode dispersion and polarization dependent loss in optical fibers," Opt. Commun., **142,** 119–125 (1997).
22. P. Lu, L. Chen and X. Bao, "Polarization mode dispersion and polarization dependent loss for a pulse in single-mode fibers," J. Lightwave Technol., **19,** 856–860 (2001).
23. B. J. Vakoc, R. M. Lanning, J. A. Tyrrell, T. P. Padera, L. A. Bartlett, T. Stylianopoulos, L. L. Munn, G. J. Tearney, D. Fukumura, R. K. Jain, and B. E. Bouma, "Three-dimensional microscopy of the tumor microenvironment in vivo using optical frequency domain imaging," Nat. Med. **15**, 1219–1223 (2009).
24. D. Waddy, L. Chen, X. Bao, "A dynamical polarization mode dispersion emulator," J. Lightwave Technol., **4,**534–536 (2003).
25. C. D. Poole, D. L. Favin, "Polarization-mode dispersion measurements based on transmission spectra through a polarizer," J. Lightwave Technol., **12,** 917–929 (1994).
26. E. Götzinger, M. Pircher, B. Baumann, C. Hirn, C. Vass, C. K. Hitzenberger, "Retinal nerve fiber layer birefringence evaluated with polarization sensitive spectral domain OCT and scanning laser polarimetry: A comparison," J. Biophoton. **1,** 129–139 (2008).
27. N. I. Fisher, T. Lewis, and B. J. J. Embleton, *Statistical Analysis of Spherical Data* (Cambridge U. Press, 1993).

1. Introduction

Optical coherence tomography (OCT) [1] resolves light scattering across depth to image biological tissue microanatomy. Polarization-sensitive OCT (PS-OCT) adds depth resolved polarimetry to extract both birefringence and tissue microanatomy [2,3]. Tissue birefringence can correlate to composition (e.g., collagen content) or functional status, and is complimentary to microanatomical imaging. Potential clinical applications of PS-OCT include retinal and anterior segment imaging in opthalmic OCT [4–7], burn depth detection in dermatology [8–10], and coronary plaque characterization in intravascular OCT [11, 12]. Because of high polarimetry noise, fiber-based PS-OCT has not yet been adopted into clinical practice. Efforts to understand and mitigate this noise have identified contributions from speckle, multiple scattering, and polarization-mode dispersion (PMD). These analyses, however, lack a quantitative framework for comparing the relative importance of each [8, 13–16] and are sometimes highly specific to single implementation or algorithm and from which it is difficult to extract a more general understanding.

In this paper, we analyze in generalized terms the ability of fiber-based OCT systems to perform accurate depth-resolved polarimetry in turbid media. We show that PMD introduced

#148363 - $15.00 USD Received 1 Jun 2011; revised 1 Jul 2011; accepted 11 Jul 2011; published 15 Aug 2011

into the system by optical fiber and optical fiber devices combines with diffuse scattering to induce a significant polarimetry noise. We quantify this noise as a function of system PMD, and compare it to the signal-to-noise ratio limited noise performance. We demonstrate that PMD-induced noise dominates SNR effects in most imaging conditions, and PMD minimization should therefore be a central goal in PS-OCT instrument design and optimization. Finally, we highlight statistical properties of PMD-induced noise that inform the design of filtering algorithms which mitigate the noise induced by PMD that cannot be physically removed from the system.

2. Polarization-sensitive OCT instrumentation

PS-OCT systems include two arrangements that are optional in conventional OCT systems: a polarization-diverse receiver and a polarization-modulated sample illumination. The later is not strictly necessary but is typically included in fiber-based systems to improve extraction of birefringence of arbitrary orientations, while the former is fundamental to the ability of the instrument to perform depth-resolved polarimetry on backscattered light. Figure 1 presents the design of a polarization-sensitive system based on optical frequency domain imaging. Interference fringes are detected on each of the two orthogonal polarization channels, digitized, wavelength-resampled, and Fourier-transformed according to standard processing approaches [17]. This yields depth-resolved measurement of the backscattered field (amplitude and phase) in each orthogonal polarization state.

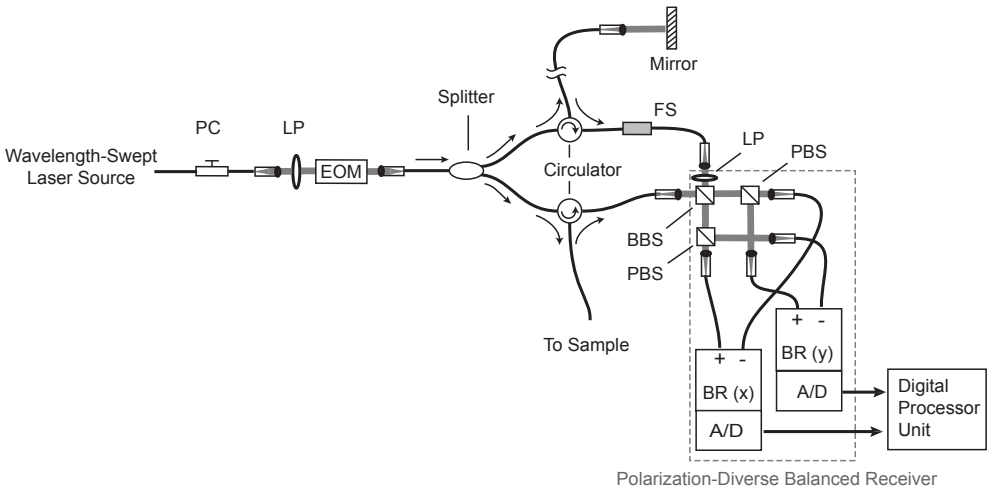

Fig. 1. Experimental setup of a polarization-sensitive optical frequency domain imaging (PS-OFDI) system. PC: polarization controller; LP: linear polarizer; EOM: electro-optical modulator; FS: frequency shifter; BBS: broad beamsplitter; PBS: polarization beamsplitter; BR: balanced receiver; A/D: analog-to-digital converter.

The polarization of backscattered light can be represented either in the Jones or Stokes formalism. In this work, we will use the Stokes formalism to describe and graphically represent polarization states and noise; the conclusions however are equally applicable to systems operating based on the Jones calculus. In the Stokes formalism, the state of polarization is given as a four-element vector $S(z)$, defined as

#148363 - $15.00 USD Received 1 Jun 2011; revised 1 Jul 2011; accepted 11 Jul 2011; published 15 Aug 2011

$$S(z) = \begin{pmatrix} I(z) \\ Q(z) \\ U(z) \\ V(z) \end{pmatrix} = \begin{pmatrix} \langle E_x(z)E_x^*(z) + E_y(z)E_y^*(z) \rangle \\ \langle E_x(z)E_x^*(z) - E_y(z)E_y^*(z) \rangle \\ \langle E_x(z)E_y^*(z) + E_x^*(z)E_y(z) \rangle \\ \langle j(E_x(z)E_y^*(z) - E_x^*(z)E_y(z)) \rangle \end{pmatrix} \quad (1)$$

where $E_x(z)$ and $E_y(z)$ are the complex fields scattered at depth z. In this work, we quantify polarimetry noise of a set of N Stokes vectors using a spherical variance metric [18], $\hat{\sigma}$,

$$\hat{\sigma} = 1 - \frac{1}{N}\sqrt{\left(\sum_{i=1}^{N}\frac{Q_i}{I_i}\right)^2 + \left(\sum_{i=1}^{N}\frac{U_i}{I_i}\right)^2 + \left(\sum_{i=1}^{N}\frac{V_i}{I_i}\right)^2} \quad (2)$$

This spherical variance ranges from 0 to 1 with the extreme values representing fully aligned and fully dispersed Stokes measurements, respectively. We note that Stokes spherical variance is closely related to the degree of polarization uniformity (DOPU) which has been used to quantify depolarizing effects in the human retina [19] and is related to an angular standard deviation measure used in Ref. [16]. Sources of polarimetry noise include depolarization effects of multiple scattering in the sample, measurement SNR, and instrumentation-induced noise. The later is the focus of this work.

3. Effect of instrument polarization-mode dispersion on polarimetry noise

PMD describes the differential propagation time of orthogonally polarized light. In an OCT system, PMD is induced by imperfections in single mode fiber or by discrete optical devices such as circulators. The presence of PMD in an OCT system interferometer causes a divergence in the complex point-spread function (PSF) of the X and Y polarization-diverse receiver channels. Consider for example a simple scenario where a PS-OCT system includes PMD aligned to the polarization axis of the receiver, i.e., wherein light transmitted to the X-channel travels a longer optical path than that of light transmitted to the Y-channel. Therefore PSFs from X and Y channels are misaligned along depth profile, i.e. there is a delay offset between X and Y channels in the presence of PMD. When imaging a mirror, this offset causes a spurious rotation of the measured Stokes vector across the mirror PSF. When imaging in turbid media, this offset decorrelates the signals $E_x(z)$ and $E_y(z)$ in a non-deterministic manner, inducing a noise in each measurement of the Stokes vectors (Fig. 2).

To estimate the significance of noise induced by a given PMD level, we can compare the induced offset in PSF depth to the system axial resolution. For fiber-induced PMD, standard single-mode fiber contains non-zero birefringence which can integrate over long lengths of fiber to produce measurable PMD. Because the orientation of the birefringence varies randomly in single mode fibers (SMF) relative to the polarization of light guided by that fiber, the integrated fiber PMD scales with the square root of fiber length. Current telecommunication fibers feature PMD specifications of $0.1ps/\sqrt{km}$ within the optical window from $1.3 \sim 1.6\mu m$. At this level, ten meters of SMF in an OFDI sample arm induces approximately $0.01ps$ of PMD which equates to a double-pass path difference of $1\mu m$ between orthogonal polarization states in tissue. This is an appreciable 10-20% of most OCT imaging resolutions ($5 \sim 10\mu m$). For an optical circulator where PMD is specified as 0.05 ps per port, a combined PMD of $0.1ps$ would yield offsets equal to the axial resolution which would induce complete decorrelation between receiver channels and make polarimetry measurements almost meaningless.

4. Methods

To analyze the noise generating mechanisms in PS-OCT instrumentation, we employed optical simulations and empirical studies. These methods are described in sections 4.1 and 4.2

#148363 - $15.00 USD Received 1 Jun 2011; revised 1 Jul 2011; accepted 11 Jul 2011; published 15 Aug 2011

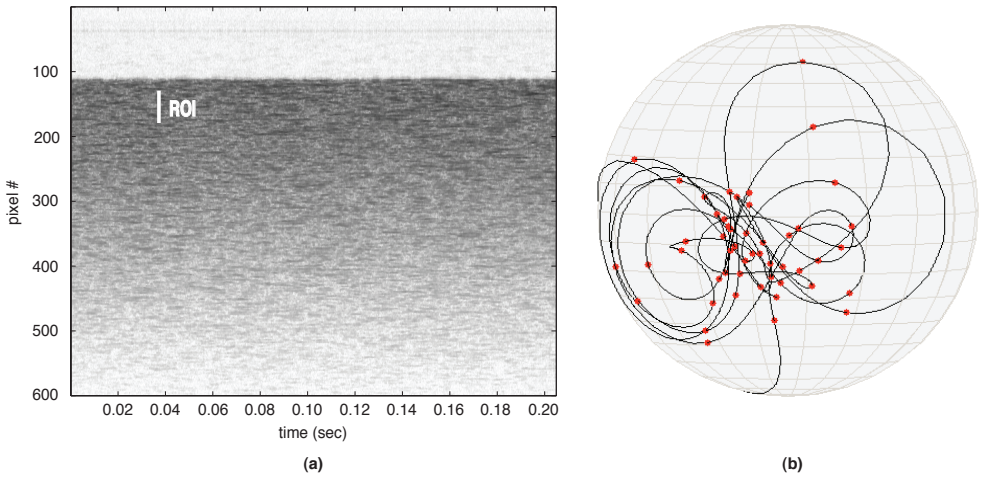

Fig. 2. (a) Structural (conventional) OFDI M-mode image of 0.5% intralipid. (b) The variation of the measured Stokes vector of backscattered light in the indicated ROI is displayed on the Poincar sphere. The random walk is caused by PMD in the instrumentation.

respectively.

4.1. Simulation of PS-OFDI noise

We developed a semi-analytic model of a PS-OFDI system (Fig. 3). We note that PMD located within the reference arm does not induce noise if a terminal polarizer is employed as shown in Fig. 1. The effect of this polarizer is to define a fixed state of polarization at this location for all wavelengths, and thus to ensure a uniform reference arm polarization at each receiver (assuming the optical components in the receiver do not induce polarization-dependent effects). The model therefore includes only the sample arm which is separated into three components: the sample arm fiber transfer function; the sample reflection function, and the interference signal generation including addition of background noise. The implementation of each of these components is described in the following sections.

4.1(a) Sample arm fiber transfer function

The sample arm transfer function describes the evolution of the light from the laser source to the sample and from the sample to the receiver. This was calculated in the presence of arbitrary birefringence, and as a function of wavelength. We started with light output from the laser and assumed it to be at a fixed state of polarization for all wavelengths. The light traveled a birefringence path described by the Jones matrix J_1 to the optical circulator (or equivalent optical splitter). The birefringent path from the circulator to the sample was described by Jones matrix J_2, and the return path by J_2^T as given by the Joness reversibility theorem [20]. Lastly, the sample arm light was directed to the interfering coupler by a birefringent path described by J_3. We assumed that the birefringent paths described by the Jones matrices J_1, J_2, and J_3 have no PMD, i.e., the matrices are independent of optical frequency. PMD within the system is included within the transfer function of the circulator (or equivalent optical splitter). The circulator was modeled by separate Jones matrices for the path from port 1 to 2, and for port 2 to 3. We denote these matrices as $T_{1\rightarrow 2}$ and $T_{2\rightarrow 3}$ respectively, where each is defined as a function of optical frequency to allow inclusion of PMD. The Jones matrix $T(\omega)$ of a birefringent

#148363 - $15.00 USD Received 1 Jun 2011; revised 1 Jul 2011; accepted 11 Jul 2011; published 15 Aug 2011

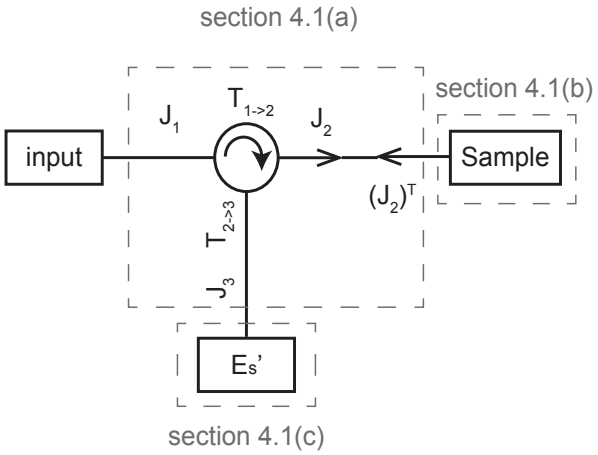

Fig. 3. Modeling of the transfer of light through the sample arm is broken into three separable stages: fiber transfer functions (described in section 4.1(a)); sample reflection (section 4.1(b)); and interference and detection (section 4.1(c)).

component was written as [21, 22].

$$T(\omega) = \exp\left(-i\vec{\beta}\omega \cdot \frac{\vec{\sigma}}{2}\right) = \begin{pmatrix} 1 & 0 \\ 0 & 1 \end{pmatrix} cos\left(\frac{\beta}{2} \cdot \omega\right) - i(r_Q\sigma_1 + r_U\sigma_2 + r_V\sigma_3) sin\left(\frac{\beta}{2} \cdot \omega\right) \quad (3)$$

where ω is the optical angular frequency, $\vec{\beta} = \beta\hat{r} = \beta\left[r_Q, r_U, r_V\right]$ is the birefringence vector of the circulator in Stokes space, i.e., the vector $\vec{\beta}$ is orientated along fast axis with its amplitude equal to the group delay difference between fast and slow axes, and $\vec{\sigma} = \left[\sigma_1, \sigma_2, \sigma_3\right]$ are the Pauli matrices [22]. In this analysis, we neglected the polarization independent time delay and loss, and we assumed negligible polarization dependent loss. In addition, we assumed only first order PMD, i.e. $\vec{\beta}$ is assumed constant over optical bandwidth of the laser.

4.1(b) Sample scattering function

To express the optical scattering of the light from turbid media, we constructed an array of $n = 1000$ scatters each positioned randomly across a $1mm$ depth range. The optical scattering that results can then be expressed as

$$E_{out}(k) = \left(\sum_{j=1}^{n} e^{2ikz_j}\right) I \cdot E_{in}(k) \quad (4)$$

where $k = 2\pi/\lambda$ is the wavenumber, z_j is the depth location of the j^{th} scatter, I is the 2x2 identity matrix, and $E_{in}(k)$ is the incident Jones vector. As stated previously, we assumed polarization-independent scattering. For a mirror signal, we used the same formalism with a single scatterer $(n = 1)$.

4.1(c) Interference, depth sectioning, and background noise addition

Using the results of sections 4.1(a) and 4.1(b), the transmission of the interferometer and the scattering function can be combined to give the sample arm light at the interfering coupler,

#148363 - $15.00 USD Received 1 Jun 2011; revised 1 Jul 2011; accepted 11 Jul 2011; published 15 Aug 2011

$E_s(k)$,

$$E_s(k) = \left(\sum_{j=1}^{n} e^{2ikz_j}\right) J_3 \cdot T_{2\to 3} \cdot J_2^T \cdot I \cdot J_2 \cdot T_{1\to 2} \cdot J_1 \cdot E_{in}(k) \tag{5}$$

The sample arm light was then interfered with the reference arm light, $E_r(k)$, which was assumed to have a wavelength-independent 45° linear polarization state. The reference arm power was set to be much larger than that of the sample arm. The current of the dual-balanced detectors was calculated as

$$i_d \propto |E_s + E_r|^2 - |E_s - E_r|^2 \tag{6}$$

Depth-resolved reflection profile $E_x(z)$ and $E_y(z)$ were obtained via Fourier transform of Eq. (6) at each of two orthogonal channels according to standard Fourier-domain processing [17]. Finally, a complex zero-mean Gaussian white noise was added to the Fourier transformed signal. In OFDI systems, this noise results from a combination of intensity noise, shot noise, or incoherent beating of sample arm reflections with reference arm light. By setting the standard deviation of the Gaussian distribution from which the noise terms were sampled, the signal to noise ratio (SNR) of the measurement was controlled.

4.2. Empirical measurements of PS-OFDI polarimetry noise

The technical details of the OFDI system used in this study are described in Ref. [17,23] and the system topology is presented in Fig. 1. Briefly, A-line scans were acquired at a rate of $50kHz$, with $6\mu m$ axial resolution in tissue and a ranging depth of $6mm$. The sensitivity of the OFDI system was measured to be $103dB$. The sample arm of the interferometer was modified to use either a circulator or a $50/50$ fused coupler to couple to the bidirectional imaging fiber. Optical powers launched to the sample via a circulator and a coupler were measured to be $11mW$ and $7mW$, respectively. The reference arm was polarized at 45° immediately prior to recombination with the sample arm light. The electro-optic polarization modulator (EOM) was not included during Stokes measurements in this study.

Imaging of calibrated mirrors and intralipid samples was performed. For the intralipid sample, the measured noise was observed to vary as a function of intralipid concentration due to competing effects of (i) low SNR at low concentrations and (ii) increased multiple scattering at higher concentrations. To minimize the combined noise, we used an empirically optimized intralipid concentration of 0.5%.

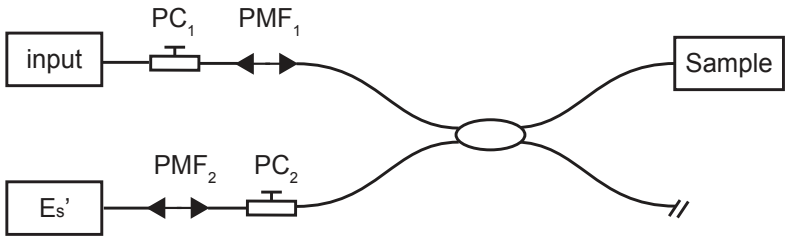

Fig. 4. Fiber patchcords containing lengths of polarization maintaining fiber (PMF) (or a length-matched SMF patchcord) were inserted into the sample arm to induce known PMD in the PS-OFDI system. PC: polarization controller.

PMD was induced by insertion of highly birefringent polarization maintaining fiber (PMF) into the sample arm [24]. In our system, we used PANDA PMF (Thorlabs PM1300-HP) which gives a beat length of less than $4mm$ at $1300nm$. The fiber was calibrated in our laboratory to yield $0.1ps$ PMD in $6.2cm$ of length. We constructed patchcords with PMDs of $0.02ps$,

#148363 - $15.00 USD Received 1 Jun 2011; revised 1 Jul 2011; accepted 11 Jul 2011; published 15 Aug 2011

$0.08ps$, and $0.16ps$. The levels of PMD were confirmed by cross-polarized analysis of spectral transmission [25]. Conventional SMF patchcords of matching lengths were also constructed. The PMD patchcords could be inserted in either of the unidirectional arms of the sample arm, i.e., on ports 1 and 3 of the coupler (Fig. 4).

5. Model validation

5.1. Relationship between SNR and Stokes variance

We first analyzed the polarimetry noise induced by the finite measurement SNR. We used the simulation described in section 4.1 with a single scatterer as a proxy for a mirror. Gaussian noise was added to the resulting signals at varying levels inducing SNRs from $0dB$ to $60dB$ at a $5dB$ interval. SNR was calculated from plotted reflectance profiles graphically as illustrated in Fig. 5(a). We then calculated the Stokes parameters using Eq. (1). The Stokes variance was calculated by repeating this for 1000 randomly generated noise signals. The dependency of Stokes variance on SNR is plotted in Fig. 5(b) and was found to follow

$$\hat{\sigma} = 1 - exp\left(\frac{1}{SNR - 1}\right) \tag{7}$$

where the SNR is defined as that measured according to the procedure illustrated in Fig. 5(a), i.e., is defined as the ratio of signal and noise power to noise power and can differ from theoretical definitions of SNR at low SNRs. To confirm these results empirically, we measured the Stokes vectors in the PS-OFDI system with a mirror sample. A variable neutral density (ND) filter was inserted in front of the mirror to allow attenuation of the signal magnitude and variation of the resulting SNR over the range of $0dB$ to $60dB$. At each setting of the ND filter and sample arm polarization controller (PC), 1024 A-lines were acquired for analysis. Data was acquired over 10 random PC states at each SNR, in order to minimize the effect from polarization sensitive components in the system. In Fig. 5(b), the mean Stokes variance and spread of Stokes variances across PC states are plotted as a function of SNR as closely match the predictions of the model.

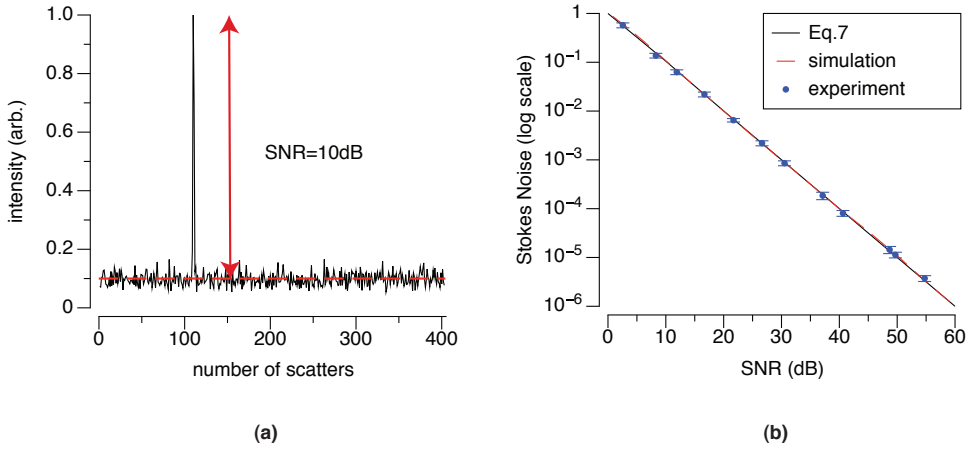

Fig. 5. (a) Measurement of signal SNR. (b) The relationship between Stokes variance and measurement SNR.

#148363 - $15.00 USD Received 1 Jun 2011; revised 1 Jul 2011; accepted 11 Jul 2011; published 15 Aug 2011

5.2. *Relationship between PMD and Stokes variance*

To quantify the polarimetry noise induced by PMD in the model, we used a diffuse scattering sample, assumed a single PMD segment, $T_{2\rightarrow3}$, and ignored SNR effects, i.e., did not add background noise. Because accumulated PMD depends on the relative orientation of the PMD axis and the launched light polarization state, noise at specific PMD levels were simulated across 10,000 random Jones matrices, J_1, J_2, and J_3. The mean and standard deviation of the resulting Stokes variance were calculated as a function of the magnitude of the PMD (Fig. 6).

To validate these results, we measured polarimetry noise from the 0.5% intralipid scattering phantom. Here, the optical circulator was removed from this system to eliminate its PMD and replaced by a fused coupler as described in section 4.2. The PM fiber patchcord was added at Port 3 to induce the discrete and calibrated PMD as modeled by $T_{2\rightarrow3}$. Measurements were acquired for each patchcord across 10 random states of PC_1 and PC_2 (see Fig. 4). The mean and standard deviation of the Stokes variance across these 10 random PC states were calculated, and match the model at all points except for PMD = $0ps$. We attribute the higher measured noise of this point to the presence of residual SMF PMD in the interferometer. This is discussed further in section 6.3.

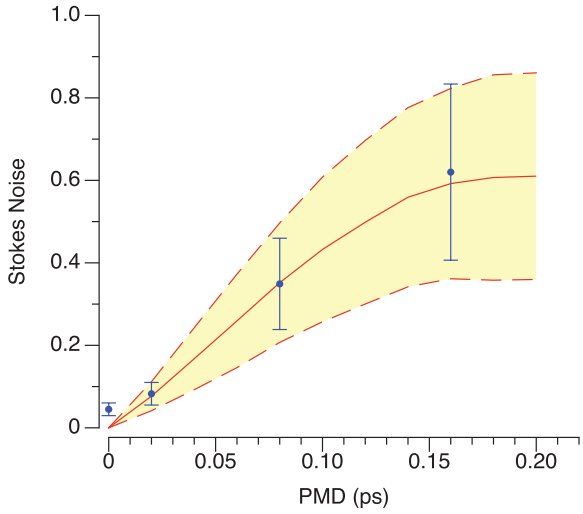

Fig. 6. The polarimetry noise induced by a single PMD segment. The mean (solid red curve) and standard deviation (dashed red curve, measured across Jones matrices J_1, J_2, and J_3) of the Stokes noise is plotted versus the magnitude of the PMD. Experimental mean and standard deviation Stokes noise (across 10 random states of polarization controllers PC_1 and PC_2, see Fig. 4) are plotted in blue. Noise was measured across 100 pixel depth $\times$ 10240 a-line ROIs within the speckle field.

6. Analysis and implications

In Sections 4 and 5, we described and validated the methods used to analyze the noise induced by finite SNR and non-zero PMD in PS-OFDI systems. Furthermore, the results summarized in Figs. 5 and 6 provide guidance on the impact of SNR and PMD in measured polarization noise. In this section, we use these tools to further analyze the role of PMD in PS-OCT noise and discuss implications on system construction and optimization.

#148363 - $15.00 USD Received 1 Jun 2011; revised 1 Jul 2011; accepted 11 Jul 2011; published 15 Aug 2011

6.1. PS-OFDI system design

OCT systems at $1.3\mu m$ commonly use optical circulators in the sample and reference arms to reduce loss and increase sensitivity. To analyze the impact of circulators on polarimetry measurements, the reduction in noise due to SNR improvement must be compared to the increase in noise due to circulator PMD. To analyze this, simulations were performed for varying per-path PMD (parameters $T_{1\to1}$ and $T_{2\to3}$) and 10,000 random combinations of Jones matrices J_1, J_2, and J_3. The resulting noise is plotted in Fig. 7(a) as a function of the per-path PMD level. Assuming PMD levels in SMF at $0.1ps/\sqrt{km}$, the noise induced by SMF within the sample arm can be estimated by lumping this distributed PMD into the a single location, i.e., $T_{2\to3}$ (as analyzed by Fig. 6). Using this model, the relationship between sample arm optical fiber length PMD-induced noise was calculated (Fig. 7(b)).

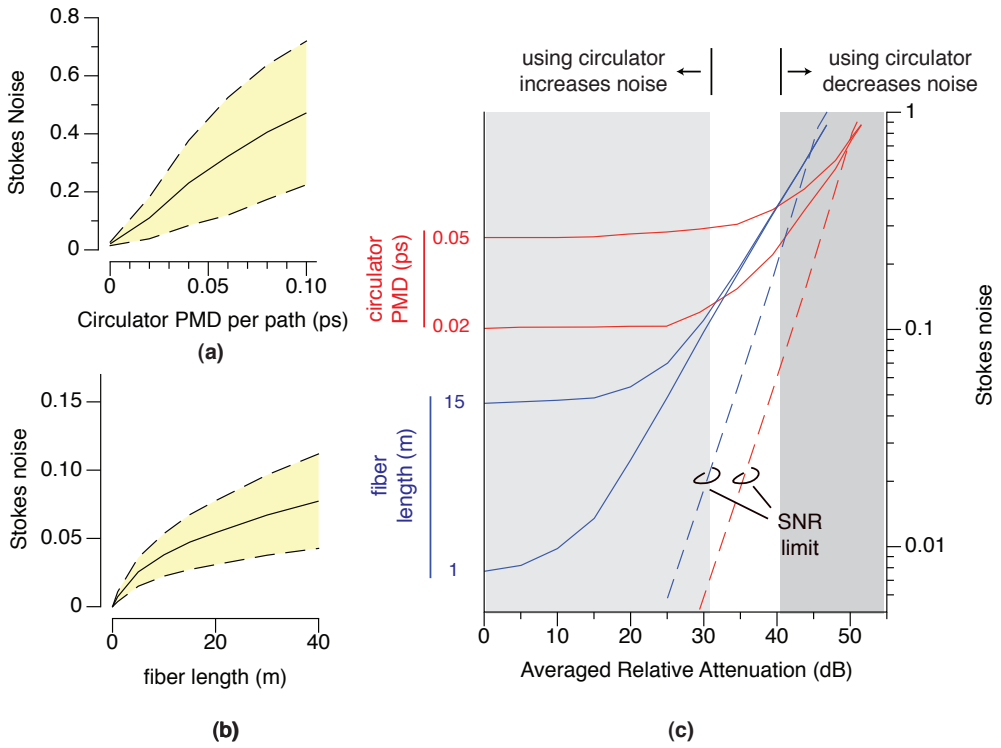

Fig. 7. Analysis of the impact of a circulator on polarimetry noise. (a) The noise induced by inclusion of a circulator in the sample arm is plotted as a function of the per-path PMD of the circulator. The mean (solid) and spread (standard deviation, dashed line) are calculated across random birefringence in the fiber leads of the circulator. (b) The noise induced by SMF PMD (assuming a circulator is not used) is plotted as a function of the SMF optical length. An average PMD level of $0.1ps/\sqrt{km}$ was assumed. (c) The total polarimetry instrumentation noise (solid curves) versus signal attenuation for systems including a circulator (red) and a fused coupler (blue). Measurement SNRs of $50dB/46dB$ were assumed for a signal attenuation of $0dB$ with and without the circulator. The contribution of measurement SNR alone is presented as dashed lines.

Combining the results of Fig. 7(a-b) with the relationship between SNR and noise (Eq. 7), we can analyze the impact of a circulator on PS-OCT noise. In Fig. 7(c), the Stokes noise is

#148363 - $15.00 USD Received 1 Jun 2011; revised 1 Jul 2011; accepted 11 Jul 2011; published 15 Aug 2011

plotted as a function of signal attenuation with and without use of a circulator. In the later case, the SNR for a given signal attenuation is assumed $4dB$ higher. The SNR at the 0 dB attenuation (i.e., tissue surface) was set at $50dB/46dB$ with/without inclusion of the circulator. The signal attenuation axis can be interpreted as an approximate proxy for imaging depth. Figure 7(c) provides curves for differing levels of circulator PMD and differing lengths of SMF. These results demonstrate that the use of a circulator largely degrades polarimetry performance, with meaningful improvements in polarimetry noise occurring only from highly attenuated (deep) signals. We note that this analysis neglects the effects of multiple scattering which is likely to play a role in polarimetry noise acquired at deeper locations. Without a circulator, it is expected that Stokes noise can be reduced, although it is unlikely that SNR limited Stokes measurements can be made for SNRs exceeding $20dB$ due to the effects of SMF PMD. Minimal length of low PMD SMF should therefore be used to minimize instrumentation polarimetry noise.

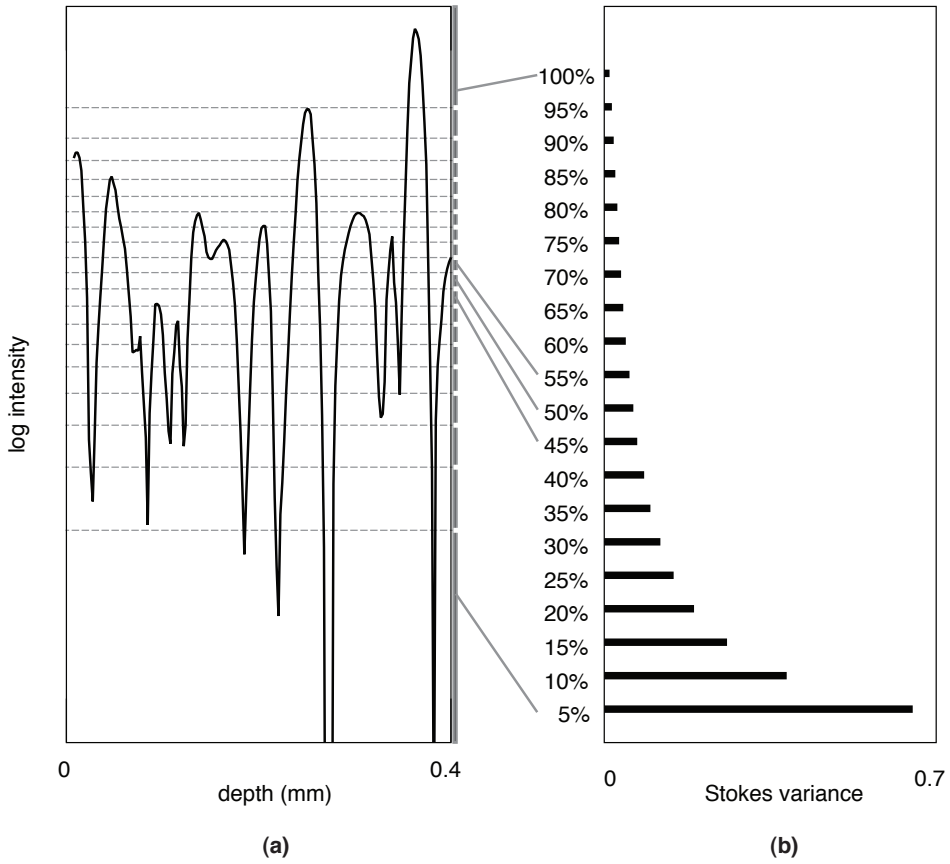

Fig. 8. Stokes noise levels induced by PMD correlate to signal intensity relative to ensemble mean intensity. (a) A section of a single A-line generated from the modeling. The intensity quantiles at 5% spacing are highlighted. (b) Stokes spherical variance calculated within each quantile shows significant dependence on relative local intensity, suggesting signals from the lower two quantiles should be discarded in any quantification or image generation algorithm.

#148363 - $15.00 USD Received 1 Jun 2011; revised 1 Jul 2011; accepted 11 Jul 2011; published 15 Aug 2011

6.2. *Reduction of Stokes noise through filtering*

In some clinical applications it is not possible to significantly reduce fiber length. In cardiovascular imaging, for example, significant fiber lengths are needed to construct the intravascular catheter ($\sim$1.5 meters physical, 3 meters double pass) and rotary coupler ($\sim$3 meters physical, 6 meters double pass). These combine with several meters of system fiber. In these applications, methods for processing signals to minimize noise originating from residual PMD would be of value.

Prior works have used absolute intensity thresholding to reduce PS-OCT noise; signals with SNRs below a given threshold are discarded [26]. However, the small regime over which PS-OCT noise are SNR limited (see Fig. 7) suggests this approach may be ineffective over the majority of the image space.

We used modeling to explore statistical dependencies between signal amplitude and PMD-induced Stokes measurement noise in the absence of added noise, i.e., with infinite SNR. Linear polarized light was launched at 45° to a small PMD ($0.02ps$) oriented at 0°. The intensity quantile lines at 5% resolution as derived from 10,000 speckle randomized A-lines were calculated, and Stokes variance was calculated separately within each quantile (Fig. 8). It can be seen that for PMD-induced noise, Stokes variance correlates closely with signal amplitude (relative to ensemble average amplitude). Note that in this simulation, SNR is infinite and this result describes the correlation of Stokes measurements to local speckle amplitude and is not an SNR effect. Stated alternatively, polarization measurements at local speckle peaks are far more accurate than those of speckle nulls regardless of the absolute signal SNR.

This result suggests filtering or estimation algorithms that use a weighting derived from local intensity (i.e, relative to ensemble averaged intensity). We explored the performance of five candidate algorithms (Table 1). To evaluate performance, groups of 20 measurements were selected randomly from the 10,000 simulated A-lines, and a single Stokes vector was extracted from each group using each of the five estimation algorithms. The error was quantified as the mean angle between the estimated Stokes vector and the input Stokes vector (45°) across 1000 groups. For intensity agnostic algorithms, spherical median outperforms mean estimation. For intensity weighted algorithms (i.e., maximum, trimmed mean, weighted mean), the weighted mean performs optimally. Many other estimators are possible that may further improve performance and can be integrated into PS-OCT algorithms to mitigate the effect of residual PMD. Note that to implement intensity weighted estimation, methods for estimating the local average intensity from the image data are required.

7. Conclusion

We have developed and validated methods for quantifying the impact of instrument PMD on depth-resolved polarimetry in OCT. Using these tools, we have demonstrated that small levels of PMD induced by circulators and even by moderate lengths of single-mode optical fibers are likely to be a dominating source of instrumentation noise in fiber-based PS-OCT systems. It was shown that inclusion of circulators likely worsens polarization noise performance, despite its benefit in SNR. Finally, a correlation between polarization measurement noise and local intensity was shown, and the use of this correlation in filtering and estimation algorithms was demonstrated to improve performance relative to conventional mean filtering.

The analysis of this work assumes non polarization-maintaining single mode fibers. The use of polarization-maintaining fiber may be a solution by controlling precisely the launched polarization. However, PM fiber couplings (either by connector or splice) will not be perfectly aligned. The impact of these imperfections needs to be studied to reveal whether the use of PM fiber increases or decreases PMD-induced noise. A more practical solution may be to implement methods for measuring the PMD within the instrumentation and removing its effect in

#148363 - $15.00 USD Received 1 Jun 2011; revised 1 Jul 2011; accepted 11 Jul 2011; published 15 Aug 2011

Table 1. Comparison of Estimation Methods Operating on PMD-induced Polarimetry Noise*

Algorithm	Expression	Estimation
Mean	$\hat{S} = (1/N)\sum_{i=1}^{N} \vec{S}_i$	94 *mrad*
Spherical median [27]	$\hat{S} : min \sum_{i=1}^{N} \arccos(\hat{S} \cdot \vec{S}_i)$	76 *mrad*
Maximum	$\hat{S} = \vec{S}_N$	147 *mrad*
Trimmed mean	$\hat{S} = (2/N)\sum_{i=(N/2+1)}^{N} \vec{S}_i$	77 *mrad*
Weighted mean	$\hat{S} = (1/N)\sum_{i=1}^{N} (\vec{S}_i/\sigma_i)$, where $\sigma_i = fct(I_i/\langle I \rangle)$	60 *mrad*

*Sets of N measurements, $S = (S_1, S_2, ...S_N)$, were arranged in rank order according to their associated intensities, $I_1 < I_2 < ... < I_{N-1} < I_N$. The estimated Stokes vector, $\hat{S}$, was derived from this rank order set using either intensity agnostic (mean, spherical median) or intensity weighted algorithms.

post-processing. This is a solution that we are actively pursuing.

Finally, it is important to again emphasize that this noise analysis is confined to instrumentation noise and does not include the effect of scattering-induced noise within the sample. For some applications, sample-induced noise is dominating, and the importance of PMD and other instrumentation sources of noise is therefore lessened. Because tissue properties vary significantly across applications, analyses of sample-induced versus instrument-induced noise in PS-OCT will need to be performed separately for each application.

Acknowledgement

We would like to thank Zhongxi Zhang at University of Ottawa for valuable discussion on simulation of polarization mode dispersion. This research was supported in part by US National Institutes of Health grant K25-CA127465 and Center for Integration of Medicine & Innovative Technology (CIMIT).

#148363 - $15.00 USD Received 1 Jun 2011; revised 1 Jul 2011; accepted 11 Jul 2011; published 15 Aug 2011